

The [Fe IV] Discrepancy: Constraining the Iron Abundances in Nebulae

Mónica Rodríguez

*Instituto Nacional de Astrofísica, Óptica y Electrónica, INAOE,
Apdo Postal 51 y 216, 72000 Puebla, Pue., Mexico*

mrodri@inaoep.mx

Robert H. Rubin¹

NASA Ames Research Center, Moffett Field, CA 94035-1000

rubin@cygnus.arc.nasa.gov

ABSTRACT

We study the current discrepancy between the model-predicted and measured concentrations of Fe^{++} and Fe^{3+} in ionized nebulae. We calculate a set of photoionization models, updated with the atomic data relevant to the problem, and compare their results with those derived for the available nebulae where both [Fe III] and [Fe IV] lines have been measured. Our new model results are closer to the measured values than the results of previous calculations, but a discrepancy remains. This discrepancy translates into an uncertainty in the derived Fe abundances of a factor up to ~ 4 . We explore the possible causes of this discrepancy and find that errors in the Fe atomic data may be the most likely explanation. The discrepancy can be fully accounted for by any of the following changes: (1) an increase by a factor of ~ 10 in the recombination rate (radiative plus dielectronic, or charge transfer) for Fe^{3+} , (2) an increase by a factor of 2–3 in the effective collision strengths for Fe^{++} , or (3) a decrease by a factor of 2–3 in the effective collision strengths for Fe^{3+} . We derive the Fe abundances implied by these three explanations and use the results to constrain the degree of depletion of Fe in our sample nebulae. The Galactic H II regions and planetary nebulae are found to have high depletion factors, with less than 5% of their Fe atoms in the gas phase. The extragalactic H II regions (LMC 30 Doradus, SMC N88A, and SBS 0335–052) have somewhat lower depletions. The metal-deficient blue compact galaxy SBS 0335–052 could have from 13% to 40% of Fe in the gas phase. The depletions derived for the different objects define a trend of increasing depletion at higher metallicities.

Subject headings: H II regions — ISM: abundances

¹Orion Enterprises

1. INTRODUCTION

The high depletion factors found for Fe in the interstellar medium (ISM), down to $\log(\text{Fe}/\text{H}) - \log(\text{Fe}/\text{H})_{\odot} = -2.3$ (Savage & Sembach 1996), and the relatively high cosmic abundance of this element, imply that Fe is a very important contributor to the mass of refractory dust grains (Sofia, Cardelli, & Savage 1994). The high depletion factors also imply that the destruction of a small quantity of dust grains will translate into a significant, i.e. measurable, increase of the Fe abundance in the gaseous phase. Hence, the study of the Fe abundance in the gas of different regions where different conditions prevail can be used to identify the processes that govern the evolution of dust in the ISM. In the diffuse ISM, the depletion patterns found for all available elements, including Fe, have led to the identification of shock waves as the main destruction mechanism of dust (Jenkins 2004 and references therein). In H II regions, the lack of strong lines from other refractory elements and the reasons outlined above imply that Fe is the best choice to study depletion trends. Such a study, based on the Fe abundances measured in several Galactic H II regions, suggests that energetic photons are responsible for the destruction of some dust grains in these nebulae (Rodríguez 1996, 2002).

Fe is expected to be in three ionization states in H II regions: $\text{Fe}/\text{H} = \text{Fe}^+/\text{H}^+ + \text{Fe}^{++}/\text{H}^+ + \text{Fe}^{3+}/\text{H}^+$, so that the measurement of Fe II, Fe III, and Fe IV emission lines will allow us to determine the Fe abundance in these nebulae. [Fe II] and [Fe III] lines, although weak, have already been observed in several H II regions and starburst galaxies (e.g. Izotov & Thuan 1999; Rodríguez 2002). Most of the optical [Fe II] lines are affected by fluorescence effects (Rodríguez 1999; Verner et al. 2000), but the Fe^+ abundance can be estimated from a few lines that are almost insensitive to fluorescence. The Fe^+ abundance turns out to be low in most of the H II regions studied to date (Rodríguez 2002), as expected from the low ionization potential for this ion (16.2 eV). On the other hand, [Fe IV] lines are much weaker than [Fe II] and [Fe III] lines and hence very difficult to observe. Therefore, the Fe abundance in H II regions is usually obtained from [Fe III] lines and an ionization-correction factor (*ICF*), derived from photoionization models, to account for the contribution of Fe^{3+} . The relation

$$\frac{\text{Fe}}{\text{O}} = ICF \frac{\text{Fe}^{++}}{\text{O}^+} = \frac{x(\text{O}^+)}{x(\text{Fe}^{++})} \frac{\text{Fe}^{++}}{\text{O}^+}, \quad (1)$$

where $x(X^{n+})$ stands for the ionization fraction of the X^{n+} ion, is especially well suited for determining the Fe abundance from optical observations of H II regions, since (1) the ionization potentials of the O and Fe ions are similar (30.6 and 54.8 eV for Fe^{++} and Fe^{3+} , 35.3 and 54.9 eV for O^+ and O^{++}), and (2) both O^+ and O^{++} can be measured from strong optical lines and one can get the O abundance $\text{O}/\text{H} = \text{O}^+/\text{H}^+ + \text{O}^{++}/\text{H}^+$, and hence also Fe/H from Fe/O . The values of the above *ICF* and their dependence, if any, with the degree of ionization can be found using grids of photoionization models. The available grids of models (Stasińska 1990; Gruenwald & Viegas 1992) imply that a constant value for this *ICF*, $x(\text{O}^+)/x(\text{Fe}^{++}) = 1.1$, should provide a good estimate of the total Fe abundance to within ± 0.2 dex.

However, available measurements of some weak [Fe IV] lines (Rubin et al. 1997; Rodríguez 2003) imply Fe^{3+} abundances that are smaller, by factors 3–8, than the values implied by equation (1) with an *ICF* equal to 1.1. This “[Fe IV] discrepancy” translates into an uncertainty of up to a factor of 5 in the Fe abundances derived for a wide range of objects, from the nearby Orion Nebula to the low metallicity blue compact galaxy SBS 0335–052. Thus, the discrepancy has important implications for our understanding of the evolution of dust in H II regions, the dependence of dust depletion factors on metallicity, and the chemical history of low metallicity dwarf galaxies.

In this paper we study the ionization equilibrium of Fe using photoionization models that incorporate recently improved values for all the atomic data relevant to the problem. We compare the new model results with the available observational data, discuss the possible reasons behind the [Fe IV] discrepancy, and study its effect on the reliability of the derived Fe abundances.

2. MODEL RESULTS

We have used the photoionization code NEBULA (see, e.g. Rubin et al. 1991a,b and references therein) to calculate a grid of spherically symmetric models of constant density ionized by a single star. We use this grid to determine the value of $x(\text{O}^+)/x(\text{Fe}^{++})$, the *ICF* in equation (1), and its dependence on the degree of ionization given by $x(\text{O}^+)/x(\text{O}^{++}) = \text{O}^+/\text{O}^{++}$.

We have updated NEBULA with the atomic data derived recently from improved calculations that are relevant to the problem: photoionization cross sections for Fe^+ , Fe^{++} , O^0 and O^+ (Nahar & Pradhan 1994; Nahar 1996a; Kjeldsen et al. 2002b; Verner et al. 1996), recombination coefficients for Fe^{++} , Fe^{3+} , O^+ and O^{++} (Nahar 1996b, 1997, 1999), the charge-exchange reactions involving these ions (Kingdon & Ferland 1996; and the ORNL/UGA Charge Transfer Database for Astrophysics¹); and the NLTE model stellar atmospheres of Sternberg, Hoffmann, & Pauldrach (2003) for solar metallicity with surface gravity $\log(g) = 4$. The photoionization cross section of Fe^+ was constructed using both the calculated values of Nahar & Pradhan (1994) and the experimental ones of Kjeldsen et al. (2002b), following the prescriptions given by the later authors. Other recent upgrades to the code are described by Simpson et al. (2004).

Our grid of 36 models covers the following parameter space: effective temperature of the ionizing star $T_{\text{eff}} = 35\,000$, $40\,000$, $45\,000$, and $50\,000$ K; total nucleon density $N = 100$, 1000 , and $10\,000$ cm^{-3} ; and “Orion metallicity” Z_{Orion} ($\text{He}/\text{H} = 0.1$, $\text{C}/\text{H} = 3.3 \times 10^{-4}$, $\text{N}/\text{H} = 4.5 \times 10^{-5}$, $\text{O}/\text{H} = 4.0 \times 10^{-4}$, $\text{Ne}/\text{H} = 8.1 \times 10^{-5}$, $\text{S}/\text{H} = 2.2 \times 10^{-5}$, $\text{Ar}/\text{H} = 4.5 \times 10^{-6}$, $\text{Si}/\text{H} = 3.0 \times 10^{-6}$, $\text{Fe}/\text{H} = 3.0 \times 10^{-6}$), $Z_{\text{Orion}}/10$, and $Z_{\text{Orion}}/30$.

All the fluxes of the ionizing stars were normalized to get a total number of ionizing photons s^{-1} for hydrogen of 10^{49} , but we checked that this has no effect on the *ICF*: we ran two new models

¹<http://www-cfadc.phy.ornl.gov/astro/ps/data/home>

with 10^{51} ionizing photons s^{-1} and found that they follow the same trend of $x(\text{O}^+)/x(\text{Fe}^{++})$ versus O^+/O^{++} defined by the original grid. This same consistent behavior was found when we used one of the supergiant models of Sternberg et al. (2003), with $T_{\text{eff}} = 40\,000$ K and $\log(g) = 3.4$, as the ionizing star.

The photoionization cross sections for the O and, especially, the Fe ions show some sharply peaked resonances arising from excitations to autoionizing states (quasi-bound states, above the ionization threshold). The energies at which these resonances occur, their widths and their peak intensities can be uncertain by a few percent or more, as seen in the direct comparison with experimental data in the few instances where the later are available (e.g. Kjeldsen et al. 2002a,b for O^+ and Fe^+ , respectively). For this reason, and for reasons of computational ease, the photoionization cross sections are usually smoothed or fitted with simple functions. We used the analytic fits of Verner et al. (1996) for O^0 and O^+ , and, following Bautista, Romano & Pradhan (1998), we smoothed the photoionization cross sections for Fe^+ and Fe^{++} doing a convolution with a Gaussian of width 3% the energy. The fluxes of the stellar atmospheres were also smoothed by convolving with a Gaussian of width 1% the energy.

Figure 1 shows the values of the *ICF* in equation (1), $x(\text{O}^+)/x(\text{Fe}^{++})$, obtained from various models as a function of the degree of ionization given by O^+/O^{++} . The results of previous ionization models (Stasińska 1990; Gruenwald & Viegas 1992) for metallicities that go from solar to 1/50 of solar, are also shown for comparison. Our new models show lower values for the *ICF*, and a small dependence with the degree of ionization. It can also be seen in Figure 1 that the results for solar or near solar metallicity show slightly larger values for the *ICF* than the results for lower metallicities. This is due to the relatively high optical depth reached in the outer parts of these solar-metallicity models at the O^+ ionization edge. At lower metallicities this optical depth becomes negligible. This dependence on the metallicity is small and will not be further considered. A least-squares fit to the new model results in Figure 1 leads to the ionization-correction scheme:

$$\frac{\text{Fe}}{\text{O}} = \frac{x(\text{O}^+)}{x(\text{Fe}^{++})} \frac{\text{Fe}^{++}}{\text{O}^+} = 0.9 \left(\frac{\text{O}^+}{\text{O}^{++}} \right)^{0.08} \frac{\text{Fe}^{++}}{\text{O}^+}. \quad (2)$$

3. COMPARISON WITH THE OBSERVATIONS

The *ICF* implied by the models can be compared with the values derived empirically for the handful of objects where the observed spectra include any [Fe IV] line (along with diagnostic lines, [O II], [O III], and [Fe III] lines). To the objects considered by Rodríguez (2003), we have added several objects where [Fe IV] $\lambda 6739.8$ has been observed recently: the H II regions M42 (Esteban et al. 2004) and NGC 3576 (García-Rojas et al. 2004), and three of the planetary nebulae (PNe) observed by Liu et al. (2004a): NGC 6210, NGC 6826, and NGC 6884. Liu et al. (2004a) provided the intensities of other [Fe IV] lines in some objects, but all of them are blends or possible misidentifications.

Physical conditions and ionic abundances have been derived following the same procedure outlined in Rodríguez (2003), except that the new values for the Fe^{3+} transition probabilities of Froese Fischer & Rubin (2004) have been used for all the objects. The Fe^{3+} abundances implied by these new data differ from the values presented by Rodríguez (2003) by less than 20%. Table 1 shows the physical conditions used in the abundance determination; Table 2 shows the ionic and total abundances derived for all the objects. In all the objects but two (N88A and SBS 0335–052), the abundances have been derived with the usual two-zone scheme: we used the electron temperature implied by the [O III] diagnostic lines, $T_e[\text{O III}]$, to derive the O^{++} and Fe^{3+} abundances, and $T_e[\text{N II}]$ to derive the O^+ and Fe^{++} abundances. In N88A and SBS 0335–052, we used $T_e[\text{O III}]$ to derive all ionic abundances. We could have used instead an uncertain estimate of $T_e[\text{N II}]$ obtained from $T_e[\text{O III}]$ and one of the existing relations between the two T_e 's (either empirical or derived from photoionization models), but this would not change our results in a significant way. For example, with the relation of Campbell, Terlevich & Melnick (1986) we obtain $T_e[\text{N II}] = 12\,900$ K in N88A bar. If we had used this T_e instead of $T_e[\text{O III}] = 14\,200$ K to derive the O^+ and Fe^{++} abundances in this object, the total Fe and O abundances presented in Table 2 would change by less than 0.05 dex, and the value of any of the ionic ratios we will be considering would remain within the error bars.

As in Rodríguez (2003), it has been assumed that $\text{O}/\text{H} = \text{O}^+/\text{H}^+ + \text{O}^{++}/\text{H}^+$, $\text{Fe}/\text{H} = \text{Fe}^+/\text{H}^+ + \text{Fe}^{++}/\text{H}^+ + \text{Fe}^{3+}/\text{H}^+$, and that the Fe^+ abundance is negligible in those objects showing a high degree of ionization. The spectra of the PNe and SBS 0335–052 show some lines from high ionization ions, such as [O IV], [Fe V], [Fe VI] or [Fe VII], but we expect that only traces of these ions are likely to be present in our sample objects. Liu et al. (2004b) calculated $\text{O}^{3+}/\text{H}^+ \sim 3 \times 10^{-5}$ from the [O IV] line at $25.9 \mu\text{m}$ measured by the Infrared Space Observatory (*ISO*) in NGC 6884. This O^{3+} abundance is just 8% of our adopted O abundance. Liu et al. also estimated that the contribution of O^{3+} to the total abundance would be ~ 10 times lower for NGC 6210 and completely negligible for NGC 6826. Furthermore, since Fe^{3+} has an ionization potential very close to that of O^{++} (54.8 and 54.9 eV, respectively), Fe^{4+} is not likely to have a significant concentration. Similar considerations, based on the $\text{He}^{++}/\text{He}^+$ ratio, were used by Rodríguez (2003) to conclude that the concentrations of O^{3+} and Fe^{4+} are likely to be very low for the other high ionization objects.

The values of $x(\text{O}^+)/x(\text{Fe}^{++})$ versus O^+/O^{++} implied by the results in Table 2 are compared with the model results in Figure 2. The new model results, although closer to the measured values than were the previous model predictions, are still unable to explain the measured values. We constructed additional models with a different geometry, where the ionized gas is located in a shell around the star. We used $Z_{\text{Orion}}/10$, $T_{\text{eff}} = 45\,000$ and $50\,000$ K, $N = 100$, 1000 , and $10\,000 \text{ cm}^{-3}$, and internal radii for the shell in the range 0.1–5.4 pc. Typical results, shown in Figure 2 as stars, are very close to those obtained from the spherical models. We also calculated the *ICF* implied by different lines of sight through the spherical model with $Z_{\text{Orion}}/10$, $T_{\text{eff}} = 45\,000$ K, and $N = 100 \text{ cm}^{-3}$. The results followed the same trend defined by the shell models, and did not help

in explaining the discrepancy. Hence, we did not pursue this approach further.

One could also speculate that the discrepancy is due to the fact that we are comparing simple constant-density models with complex real objects. Moore, Hester, & Dufour (2004) found that this can lead to significant errors in ratios like O^+/O^{++} . However, according to the models, Fe^{++} and O^+ should have similar concentrations, and [O II] and [Fe III] lines should form in similar regions in the nebula, and hence these ions should be affected by similar systematic effects.

Rodríguez (2003) discussed the most likely explanations of this discrepancy, namely, errors in the collision strengths used to derive the Fe^{++} and Fe^{3+} abundances or errors in the ICF derived from models, probably arising from errors in the input parameters governing the ionization equilibrium.

If the model-predicted ICF is seriously wrong, then the trend defined in Figure 2 by the observed objects will lead to an ICF that should be more reliable than the one predicted by the model results. The trend is only clearly defined for those objects whose degree of ionization is within the range covered by the models (i.e. with $\log(O^+/O^{++})$ above ~ -1.35). We note that since our photoionization models are tailored for H II regions, the highest T_{eff} we are considering is 50 000 K. For this T_{eff} , there are very few ionizing photons with energies above ~ 54 eV and O^{++} and Fe^{3+} (both with ionization potentials above 54 eV) are not expected to be substantially further ionized. The three objects with higher degree of ionization in Figure 2 are PNe, where the central stars can reach or surpass T_{eff} of 100 000 K. Even if these objects do not have significant concentrations of either O^{3+} or Fe^{4+} , as discussed above, they might have small amounts of these ions that could lead to a change in the trend followed by the ICF with $\log(O^+/O^{++})$. Hence, a change in the trend at $\log(O^+/O^{++}) \sim -1.4$ does not seem unlikely. Thus we limit the relationship to define an ICF for lower degrees of ionization. A least-squares linear fit to the data for those objects with $\log(O^+/O^{++}) > -1.35$ in Figure 2 leads to the ionization-correction scheme:

$$\frac{Fe}{O} = \frac{x(O^+)}{x(Fe^{++})} \frac{Fe^{++}}{O^+} = 1.1 \left(\frac{O^+}{O^{++}} \right)^{0.58} \frac{Fe^{++}}{O^+}, \quad (3)$$

which should be valid for $-1.35 < \log(O^+/O^{++}) < -0.1$. For $\log(O^+/O^{++}) \geq -0.1$, the concentrations of Fe^{++} and O^+ will grow, making these ions the dominant ionization states, and a constant ICF :

$$\frac{Fe}{O} = \frac{Fe^+ + Fe^{++}}{O^+}, \quad (4)$$

would be the preferred choice. The contribution of Fe^+ will still be very small for most objects (Rodríguez 2002). In § 4 we consider what changes in the relevant input parameters that affect the ionization equilibrium of the models would be needed to explain the discrepancy. Changes in the values of the collision strengths are considered in § 5.

4. AN ERROR IN THE MODELS' *ICF*?

The *ICF* implied by the photoionization models depends on the following factors: (1) the number of photoionizations of Fe^{++} and O^+ , which in turn depends on the photoionization cross sections for these ions and on the spectral energy distribution of the ionizing flux, (2) the number of radiative and dielectronic recombinations of Fe^{3+} and O^{++} , which depends on the recombination coefficients, and (3) the rate of the charge-exchange reactions leading to recombinations of Fe^{3+} and O^{++} .

The smoothing of the photoionization cross sections and the stellar atmospheres could introduce errors in the number of photoionizations computed in the models. In order to constrain these errors, we calculated the number of photoionizations of Fe^{++} implied by the original stellar fluxes and photoionization cross section of Fe^{++} by integrating the product of these two quantities between $h\nu_0 = 30.65$ eV, the ionization potential of Fe^{++} , and $h\nu_1 = 54.4$ eV, the ionization potential of He^+ and the maximum energy considered in the photoionization models. We compared the result with the number of photoionizations implied by the smoothed stellar fluxes and found that the original value was 1% lower than the smoothed one for $T_{\text{eff}} = 35\,000$ K and 18, 6, and 9% higher for $T_{\text{eff}} = 40\,000$, 45 000, and 50 000 K, respectively. These differences are far too small to change our results in a significant way.

We consider now the effect of changes in the stellar ionizing flux. The ionizing fluxes could be wrong because of uncertainties in the stellar atmosphere models, or because we are using the results for models with solar metallicity whereas lower metallicities might be more appropriate. We can constrain the kind of changes we need to check by noting that the smoothed photoionization cross sections for Fe^{++} and O^+ are very similar for energies above the O^+ ionization threshold (Fig. 3). Therefore, only a change in the ionizing flux in the energy range between the two ionization thresholds (i.e. between 30.65 and 35.12 eV) can have a significant effect on the *ICF*. A lower ionizing flux in this energy range will change the *ICF* in the right direction to solve the discrepancy. We did a test with two of the model atmospheres, dividing their fluxes by factors of up to a factor of ten in the energy interval of interest (see Fig. 4), thus bringing the fluxes in this interval very close to zero. We achieved this by dividing the fluxes by the function $1 + 9 \exp[-0.5((E - 2.145)/0.06)^2]$, where E is the energy in Ry. We ran two models using these new stellar fluxes (with $N = 100 \text{ cm}^{-3}$ and Z_{Orion}), and found that the decrease in the *ICF* was $\simeq 0.07$ dex, far too small to explain the discrepancy. We believe that this rules out any uncertainty in the stellar ionizing flux distributions as the main cause behind the discrepancy.

We are then left with errors in the atomic data governing the ionization equilibrium of O and Fe as the possible explanations of the discrepancy. Since the Fe ions are more complex than the O ions, their atomic data are more difficult to calculate and hence more uncertain. We will center our discussion on the effects of changes in the ionization and recombination data for Fe. Changes in the data for O going in the opposite direction from those we will consider for the Fe data would also help in explaining the discrepancy, but we note that the discrepancy was first discovered as related

to Fe by considering tailor-made models for M42, i.e., the discrepancy seems to be independent of the degree of ionization given by the O ions (Rubin et al. 1997). We consider the $\text{Fe}^{++} \longleftrightarrow \text{Fe}^{3+}$ ionization equilibrium, since Fe^+ has a low concentration in all the objects of our sample. At a given point in a nebula, the ionization-equilibrium equation for these two ions is given by (see, e.g. Osterbrock 1989):

$$N(\text{Fe}^{++}) \int_{\nu_0}^{\nu_1} \frac{4\pi J_\nu}{h\nu} \sigma(\text{Fe}^{++}) d\nu = N(\text{Fe}^{3+}) N_e \alpha(\text{Fe}^{++}, T_e) + N(\text{Fe}^{3+}) N(\text{H}^0) \delta(T_e), \quad (5)$$

where $N(X)$ is the volume density of X , J_ν is the mean intensity of the radiation field at the point, $\sigma(\text{Fe}^{++})$ is the photoionization cross section for Fe^{++} , $\alpha(\text{Fe}^{++}, T_e)$ is the total (radiative plus dielectronic) recombination coefficient of Fe^{3+} , and $\delta(T_e)$ is the rate coefficient of the charge-exchange reaction $\text{Fe}^{3+} + \text{H}^0 \rightarrow \text{Fe}^{++} + \text{H}^+$.

For a given O^+/O^{++} we can get a lower value of the *ICF* $x(\text{O}^+)/x(\text{Fe}^{++})$ by decreasing the photoionization cross section for Fe^{++} or increasing either the recombination coefficient of Fe^{3+} or the rate of the aforementioned charge-exchange reaction. We selected two models to use as templates. They are ionized by stars with $T_{\text{eff}} = 40\,000$ K and 10^{49} ionizing photons s^{-1} , and $T_{\text{eff}} = 50\,000$ K, 10^{51} ionizing photons s^{-1} ; both have $N = 100 \text{ cm}^{-3}$ and $Z_{\text{Orion}}/10$. We then tested sequentially the effect on the results of these models of changes by a factor of 2 in the photoionization cross section, and by factors of 2 and 10 in each of the recombination coefficient and the rate of the charge-exchange reaction. We did not consider a change by a factor of 10 in the photoionization cross section of Fe^{++} because the comparisons of calculated cross sections with the available experimental data (e.g. Kjeldsen et al. 2002a,b for O^+ and Fe^+ , respectively) usually show better agreement. The results from the two model templates and from the test calculations are shown as connected open circles in Figure 5, where it can be seen that a change by a factor of 10 in the recombination data will be needed in order to reproduce the observed results. A factor of 10 uncertainty would not be unexpected for the dielectronic part of a recombination coefficient or for the rate of a charge-exchange reaction (Ferland 2003).

5. ERRORS IN THE COLLISION STRENGTHS FOR Fe^{++} OR Fe^{3+} ?

Figure 6a shows the comparison between the $x(\text{O}^+)/x(\text{Fe}^{++})$ *ICF* implied by models and observations when either the derived Fe^{++} abundances are divided by a factor 2.5 or the Fe^{3+} abundances are multiplied by the same factor. Figure 6b shows the same comparison for $\text{Fe}^{++}/\text{Fe}^{3+}$ as a function of O^+/O^{++} . It can be seen that this factor of 2.5 change in the relative abundances of Fe^{++} and Fe^{3+} would lead to an agreement between observations and models. It might then look promising that the recent calculations of collision strengths for Fe^{++} by McLaughlin et al. (2002) differ from the previous results we are using here (Zhang 1996) by factors up to 2. This new atomic data might then imply Fe^{++} abundances lower by a factor of 2, thus reducing the discrepancy in Fig. 2. However, McLaughlin et al. (2002) calculate the collision strengths only for transitions between terms, whereas the fine-structure values are needed to derive Fe^{++} abundances and, most

important in the present context, to check their reliability by comparing the predicted relative line intensities with the observed ones. The atomic data we are using here for [Fe III] do seem to be reliable, since they lead to consistent abundances for the various [Fe III] lines (Rodríguez 2002, 2003) and, when the [Fe III] lines are used as an electron density diagnostic, they lead to values similar to those implied by the usual diagnostics such as [S II], [Cl III] or [Ar IV] (García-Rojas et al. 2004; Esteban et al. 2004). However, it is possible to preserve this consistency while changing the values of the collision strengths so that they lead to lower Fe^{++} abundances. Since the upper levels of the optical [Fe III] lines are mainly populated through collisional transitions from the ground term, the relative intensities of the lines we are considering will not change significantly if all the collision strengths for transitions originating in the ground term are changed by a similar factor. It is therefore suggestive that all the term-averaged collision strengths of Zhang (1996) for transitions from the ground term are lower than the results given by McLaughlin et al. (2002) by factors ~ 2 . A test calculation shows that if the collision strengths of Zhang (1996) for transitions from the ground term are enhanced by a factor of 2, the [Fe III] line ratios remain mostly unaffected and the Fe^{++} abundances are lower by a factor of ~ 2 . Hence, this change in the Fe^{++} collisional data would explain most, if not all, the discrepancy. New calculations that provide the collision strengths for the fine-structure levels will be extremely valuable in order to test this idea.

On the other hand, the discrepancy might be due to errors in the atomic data for Fe^{3+} , which are difficult to test through a comparison between observed and predicted relative line intensities because the lines are very weak and difficult to measure. Our new model results along with the new observational results for M42 and, especially, for NGC 3576 in Figure 2, which are very close to the expected ones, allow us to rule out the large uncertainties in the collision strengths, of factors 6–7, contemplated by Rodríguez (2003), and to settle for changes by factors 2–3.

A comparison between the results in Figures 5 and 6 shows that both the explanation involving errors in the collision strengths of Fe^{3+} or Fe^{++} by a factor 2–3 and the explanation requiring a change in the recombination data for Fe^{3+} (the recombination coefficient or the rate of the charge-exchange reaction with H^0) by a factor of 10 look equally plausible (it must be taken into account that the model results show some dispersion around their defined trends). Of course, the final explanation for the discrepancy might require a combination of causes, but the fact that we cannot decide on the most likely or on the more important one, introduces an uncertainty in the Fe abundances calculated for the various objects. In the next section, we assess this uncertainty and try to see what constraints we can place on the Fe abundance in the nebulae of our sample.

6. CONSTRAINING THE IRON ABUNDANCES

The last two columns in Table 2 show the Fe abundances derived for all the objects from the sum of the ionic abundances (col. [8]) and from the Fe^{++} abundance and the *ICF* (see eq. [2]) implied by our photoionization models (col. [9]). If the model predicted *ICF* is seriously wrong, the best values for the Fe abundance will be those shown in column (8); if the discrepancy is only

due to errors in the Fe^{3+} collision strengths, the best values will be those in column (9); and if the discrepancy is mainly due to errors in the Fe^{++} collision strengths by the factor of ~ 2 suggested by the calculations of McLaughlin et al. (2002) (see § 5), the best values will be those shown in column (9) lowered by ~ 0.3 dex. Figure 7 shows the depletion factors for the Fe/O abundance ratio ($[\text{Fe}/\text{O}] = \log(\text{Fe}/\text{O}) - \log(\text{Fe}/\text{O})_{\odot}$) implied by these three possibilities as a function of the O/H abundance ratio. We note that if the discrepancy is due to some combination of the aforementioned causes, the errors required in any of the atomic data are likely to be lower than those considered above, and the depletion factors will consequently be intermediate between those shown in the three panels of Figure 7. We use Fe/O to calculate depletion factors because our objects have different metallicities (see the values of the O/H abundance ratio in Table 2) but are likely to have a near solar value for Fe/O (considering the abundances in gas and dust), or at least, their intrinsic Fe/O abundance will show less variation than either O/H or Fe/H. Indeed, the Fe/O abundance ratio has been found to be near solar or slightly (~ 0.2 dex) below solar for the Magellanic Clouds and for other low-metallicity dwarf galaxies (see e.g., Venn et al. 2001; Shetrone, Côté, & Sargent (2001), and references therein). We have used $\log(\text{Fe}/\text{O})_{\odot} = -1.2$, a value that agrees to within ± 0.1 dex with recent determinations of the solar Fe and O abundances (Holweger 2001; Asplund et al. 2004; Meléndez 2004).

Even if we do not know which are the correct values for the nebular Fe abundances, several things can be inferred from the results in Figure 7. Since we are considering quite extreme variations of the atomic data entering in the abundance determinations, we can use the range of abundances as a reasonable constraint on the true Fe abundances. An inspection of the depletion factors in Figure 7 shows that the Galactic H II regions (M42, NGC 3576) and PNe (IC 4846, NGC 6210, NGC 6826, and NGC 6884) have depletion factors in the range -1.3 to -2.0 , intermediate between the values observed for warm and cold clouds in the Galactic ISM, where typical depletion factors are ~ -1.2 and ~ -2.2 , respectively (Savage & Sembach 1996). Thus most of the Fe atoms are in dust grains in these nebulae: less than $\sim 5\%$ of their total Fe abundance is present in the gas. The depletion factor in LMC 30 Doradus, where the metallicity is about 0.2 dex lower, is at the higher end of the above range, ~ -1.4 . In SMC N88A, with about 0.5 dex lower metallicity than in the Galactic objects, the depletion factor is lower, in the range -0.5 to -1.1 . The blue compact galaxy SBS 0335–052, with a metallicity -1.3 dex below those of the Galactic nebulae, shows a somewhat lower depletion, in the range -0.4 to -0.9 . The depletions could be somewhat lower for the metal-poor objects if their intrinsic Fe/O abundance ratios are below solar, as commented above. This trend of higher depletions at higher metallicities, which was also shown to hold for a smaller sample of objects by Rodríguez (2002), is consistent with what we know about depletion factors in the ISM of the Magellanic Clouds (Welty et al. 1999, 2001) and with a recent measurement of the gas to dust ratio in the SMC (Bot et al. 2004). A similar trend has been found to hold for Damped Ly α systems (Vladilo 2004). The trend could arise from a low efficiency of dust-formation processes at low metallicities or, at least for the objects in our sample, from a high dust-destruction rate due to the harsh radiation fields usually found in metal-poor galaxies. Further measurements of both [Fe III] and [Fe IV] lines in a sample of metal-poor galaxies would help to constrain this issue.

We note that the depleted Fe atoms are not likely to be in the form of silicates in N88A. Roche, Aitken, & Smith (1987) did not find the $9.7 \mu\text{m}$ silicate feature in the IR spectrum of this H II region, and Kurt et al. (1999) derived a solar value for the Si/O abundance ratio. Furthermore, Welty et al. (2001) found that Si (and Mg) are essentially undepleted in the SMC ISM, concluding that silicates cannot be an important component of dust in this galaxy. This lack of silicate dust does not seem to be a common feature of low-metallicity galaxies, since the $9.7 \mu\text{m}$ feature has been detected in SBS 0335–052 (Houck et al. 2004). The depleted Fe may be in the form of oxides or metallic grains, or deposited onto carbon grains. Such Fe-containing non-silicate dust grains are also considered to be an important dust component in our own Galaxy, where less than half of the depleted Fe can be accounted for with silicates (see Whittet 2003 and references therein).

7. SUMMARY AND CONCLUSIONS

We have presented a detailed analysis of the current discrepancy between the observationally derived and model predicted concentrations of Fe ions in ionized nebulae. We have calculated new photoionization models that incorporate state-of-the-art values for all the atomic data relevant to the problem. The predicted Fe ionic concentrations have been compared with those implied by the available observational data. Our new model results are closer to the observed values than previous calculations, but there is still a discrepancy that translates into an uncertainty in the derived Fe abundances of a factor up to 3.7. We have studied the possible reasons for this discrepancy and conclude that the most likely explanations are those due to uncertainties in the atomic data. We are able to find a satisfactory agreement between the model predictions and the observations in three different ways: (1) increasing either the total recombination coefficient or the rate of the charge exchange reaction with H^0 for Fe^{3+} by a factor of ~ 10 , (2) decreasing the collision strengths for Fe^{3+} by a factor of 2–3, and (3) increasing the collision strengths for Fe^{++} by a factor of 2–3. Of course, if errors in different atomic data are involved, the above factors need not be as large.

Since we are considering quite drastic changes in the atomic data involved in the abundance calculation, we feel justified in using the Fe abundances implied by the three possible explanations listed above as a way to constrain the true Fe abundances in the gas of our sample objects. Our set of Galactic H II regions and PNe have Fe depletion factors ($\log(\text{Fe}/\text{O}) - \log(\text{Fe}/\text{O})_{\odot}$) below -1.3 ; most of the Fe atoms are deposited onto dust grains in these nebulae. Only a few per cent or less of their Fe atoms are in the gas phase. The extragalactic H II regions of our sample (LMC 30 Doradus, SMC N88A, and SBS 0335–052) show somewhat lower depletions and help define a trend of increasing depletion with increasing metallicity (see Fig. 7). The depletion factor in SBS 0335–052, one of the most metal-deficient galaxies known, is only poorly constrained: it should be in the range -0.9 to -0.4 . The exact amount of depletion in this interesting object will not be known until the [Fe IV] discrepancy is fully explained.

We thank Janet Simpson and Grazyna Stasińska for helpful comments. The comments of

an anonymous referee also helped to improve the paper. MR acknowledges support from Mexican CONACYT project J37680-E. Support for RHR was from the NASA Long-Term Space Astrophysics (LTSA) Program and the Astrophysics Data Program (ADP). RHR thanks Scott McNealy for providing a Sun workstation. The models were run on Cray computers at NASA/Ames (Consolidated Supercomputer Management Office) and at JPL; time on the latter was provided by funding from JPL Institutional Computing and Information Services and the NASA Offices of Earth Science, Aeronautics, and Space Science.

REFERENCES

- Asplund, M., Grevesse, N., Sauval, A. J., Allende Prieto, C., & Kiselman, D. 2004, *A&A*, 417, 751
- Baldwin, J. A., Verner, E. M., Verner, D. A., Ferland, G. J., Martin, P. G., Korista, K. T., & Rubin, R. H. 2000, *ApJS*, 129, 229
- Bautista, M. A., Romano, P., & Pradhan, A. K. 1998, *ApJS*, 118, 259
- Bot, C., Boulanger, F., Lagache, G., Cambrésy, L., & Egret, D. 2004, *A&A*, 423, 567
- Campbell, A., Terlevich, R., & Melnick, J. 1986, *MNRAS*, 223, 811
- Esteban, C., Peimbert, M., García-Rojas, J., Ruiz, M.-T., Peimbert, A., & Rodríguez, M. 2004, *MNRAS*, 355, 229
- Ferland, G. J. 2003, *ARA&A*, 41, 517
- Froese Fischer, C., & Rubin, R. H. 2004, *MNRAS*, 355, 461
- García-Rojas, J., Esteban, C., Peimbert, M., Rodríguez, M., Ruiz, M.-T., & Peimbert, A. 2004, *ApJS*, 153, 501
- Gruenwald, R. B., & Viegas, S. M. 1992, *ApJS*, 78, 153
- Holweger, H. 2001, in *AIP Conf. Proc. 598, Solar and Galactic Composition*, ed. R. F. Wimmer-Schweingruber (New York: Springer-Verlag), 23
- Houck, J. R., et al. 2004, *ApJ*, 154, L211
- Hyung, S., Aller, L. H., & Lee, W.-B. 2001, *PASP*, 113, 1559
- Izotov, Y. I., Chaffee, F. H., & Schaerer, D. 2001, *A&A*, 378, L45
- Izotov, Y. I., & Thuan, T. X. 1999, *ApJ*, 511, 639
- Jenkins, E. B. 2004, in *Carnegie Observatories Astrophysics Series 4, Origin and Evolution of the Elements*, ed. A. McWilliam & M. Rauch (Cambridge: Cambridge Univ. Press), 339

- Kingdon, J. B., & Ferland, G. J. 1996, *ApJS*, 106, 205
- Kjeldsen, H., Kristensen, B., Brooks, R. L., Folkman, F., Knudsen, H., & Andersen, T. 2002a, *ApJS*, 138, 219
- Kjeldsen, H., Kristensen, B., Folkman, F., & Andersen, T. 2002b, *J. Phys. B*, 35, 3655
- Kurt, C. M., Dufour, R. J., Garnett, D. R., Skillman, E. D., Mathis, J. S., Peimbert, M., Torres-Peimbert, S., & Ruiz, M.-T. 1999, *ApJ*, 518, 246
- Liu, Y., Liu, X.-W., Luo, S.-G., & Barlow, M. J. 2004a, *MNRAS*, 353, 1231
- Liu, Y., Liu, X.-W., Barlow, M., & Luo, S.-G. J. 2004b, *MNRAS*, 353, 1251
- McLaughlin, B.M., Scott, M.P., Sunderland, A.G., Noble, C.J., Burke, V.M., & Burke, P.G. 2002, *J. Phys. B*, 35, 2755
- Meléndez, J. 2004, *ApJ*, 615, 1042
- Moore, B. D., Hester, J. J., & Dufour, R. J. 2004, *AJ*, 127, 3484
- Nahar, S. N. 1996a, *Phys. Rev. A*, 53, 1545
- Nahar, S. N. 1996b, *Phys. Rev. A*, 53, 2417
- Nahar, S. N. 1997, *Phys. Rev. A*, 55, 1980
- Nahar, S. N. 1999, *ApJS*, 120, 131
- Nahar, S. N., & Pradhan, A. K. 1994, *J. Phys. B*, 27, 429
- Osterbrock, D. E. 1989, *Astrophysics of Gaseous Nebulae and Active Galactic Nuclei* (Mill Valley: University Science Books)
- Peimbert, A. 2003, *ApJ*, 584, 735
- Roche, P. F., Aitken, D. K., & Smith, C. H. 1987, *MNRAS*, 228, 269
- Rodríguez, M. 1996, *A&A*, 313, L5
- Rodríguez, M. 1999, *A&A*, 348, 222
- Rodríguez, M. 2002, *A&A*, 389, 556
- Rodríguez, M. 2003, *ApJ*, 590, 296
- Rubin, R. H., Simpson, J. P., Haas, M. R., & Erickson, E. F. 1991a, *ApJ*, 374, 564
- Rubin, R. H., Simpson, J. P., Haas, M. R., & Erickson, E. F. 1991b, *PASP*, 103, 834

- Rubin, R. H., et al. 1997, *ApJ*, 474, L131
- Savage, B. D., & Sembach, K. R. 1996, *ARA&A*, 34, 279
- Shetrone, M. D., Côté, P., & Sargent, W. L. W. 2001, *ApJ*, 548, 592
- Simpson, J. P., Rubin, R. H., Colgan, S. W. J., Erickson, E. F., & Haas, M. R. 2004, *ApJ*, 611, 338
- Sofia, U. J., Cardelli, J. A., & Savage, B. D. 1994, *ApJ*, 430, 650
- Stasińska, G. 1990, *A&AS*, 83, 501
- Sternberg, A., Hoffmann, T. L., & Pauldrach, A. W. A. 2003, *ApJ*, 599, 1333
- Venn, K. A., Lennon, D. J., Kaufer, A., McCarthy, J. K., Przybilla, N., Kudritzki, R. P., Lemke, M., Skillman, E. D., & Smartt, S. J. 2001, *ApJ*, 547, 765
- Verner, D. A., Ferland, G. J., Korista, K. T., & Yakolev, D. G. 1996, *ApJ*, 465, 487
- Verner, E. M., Verner, D. A., Baldwin, J. A., Ferland, G. J., & Martin, P. G. 2000, *ApJ*, 543, 831
- Vladilo, G. 2004, *A&A*, 421, 479
- Welty, D. E., Frisch, P. C., Sonneborn, G., & York, D. G. 1999, *ApJ*, 512, 636
- Welty, D. E., Lauroesch, J. T., Blades, C., Hobbs, L. M., & York, D. G. 2001, *ApJ*, 554, L75
- Whittet, D. C. B. 2003, *Dust in the Galactic Environment* (Bristol: IOP Publishing)
- Zhang, H. L. 1996, *A&AS*, 119, 523

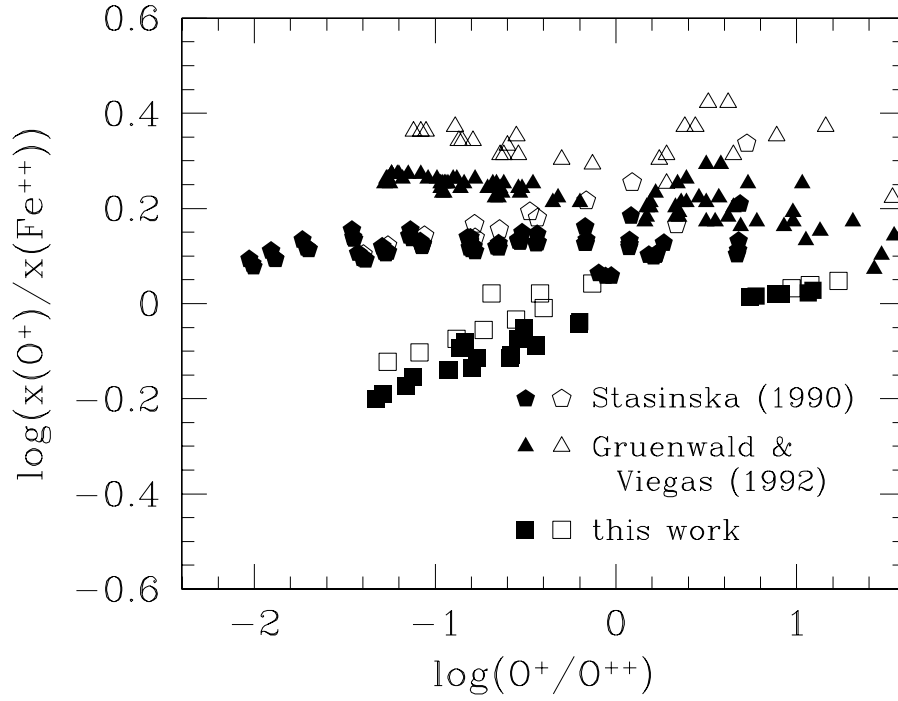


Fig. 1.— Our new model results for $x(O^+)/x(Fe^{++})$ as a function of O^+/O^{++} and the previous results by Stasińska (1990) and Gruenwald & Viegas (1992). *Open symbols:* results for solar or near solar metallicity (Z_{Orion}). *Filled symbols:* results for lower metallicities, from $Z_{\odot}/2$ to $Z_{\odot}/50$.

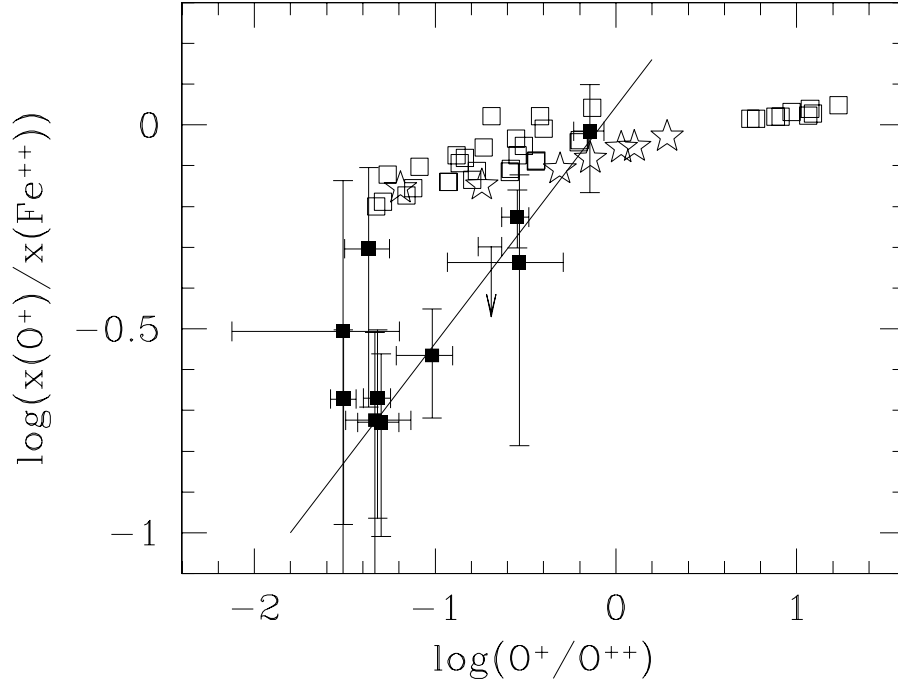


Fig. 2.— Values of $x(O^+)/x(Fe^{++})$ as a function of O^+/O^{++} for our new models and for the observed objects. *Open squares:* Results for the spherical models. *Stars:* Results for the shell models. *Filled squares:* Values calculated for the observed objects. From left to right: IC 4846 (ordinate -0.51), NGC 6826, NGC 6210, N88A square A, SBS 0335–052, NGC 6884, N88A bar, 30 Doradus (the upper limit), M42 b, M42 a, and NGC 3576. The line shows a least-squares fit to the data for those objects with $\log(O^+/O^{++}) > -1.35$.

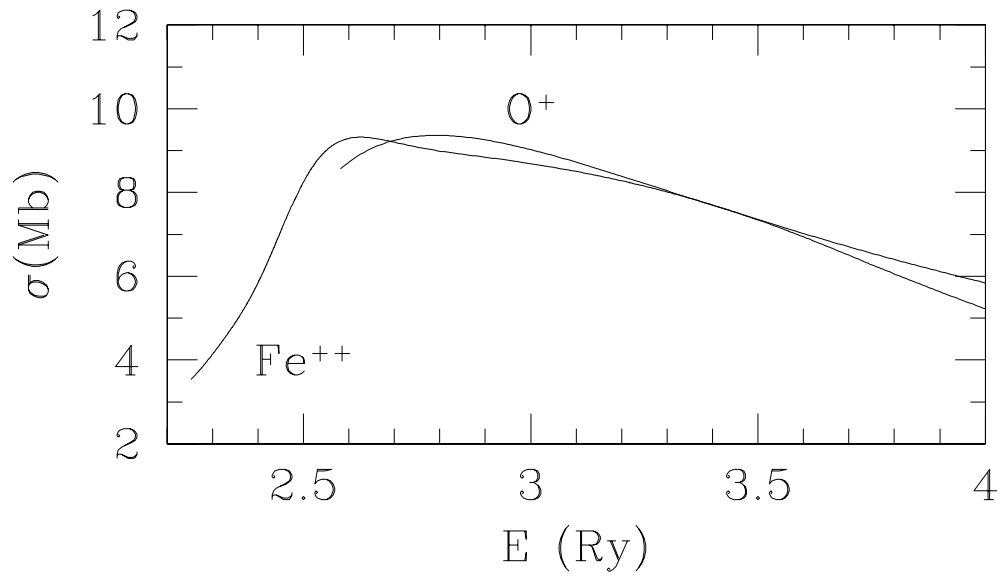


Fig. 3.— Smoothed ionization cross sections for O^+ and Fe^{++} as a function of energy. Note that they are very similar in the energy range they have in common.

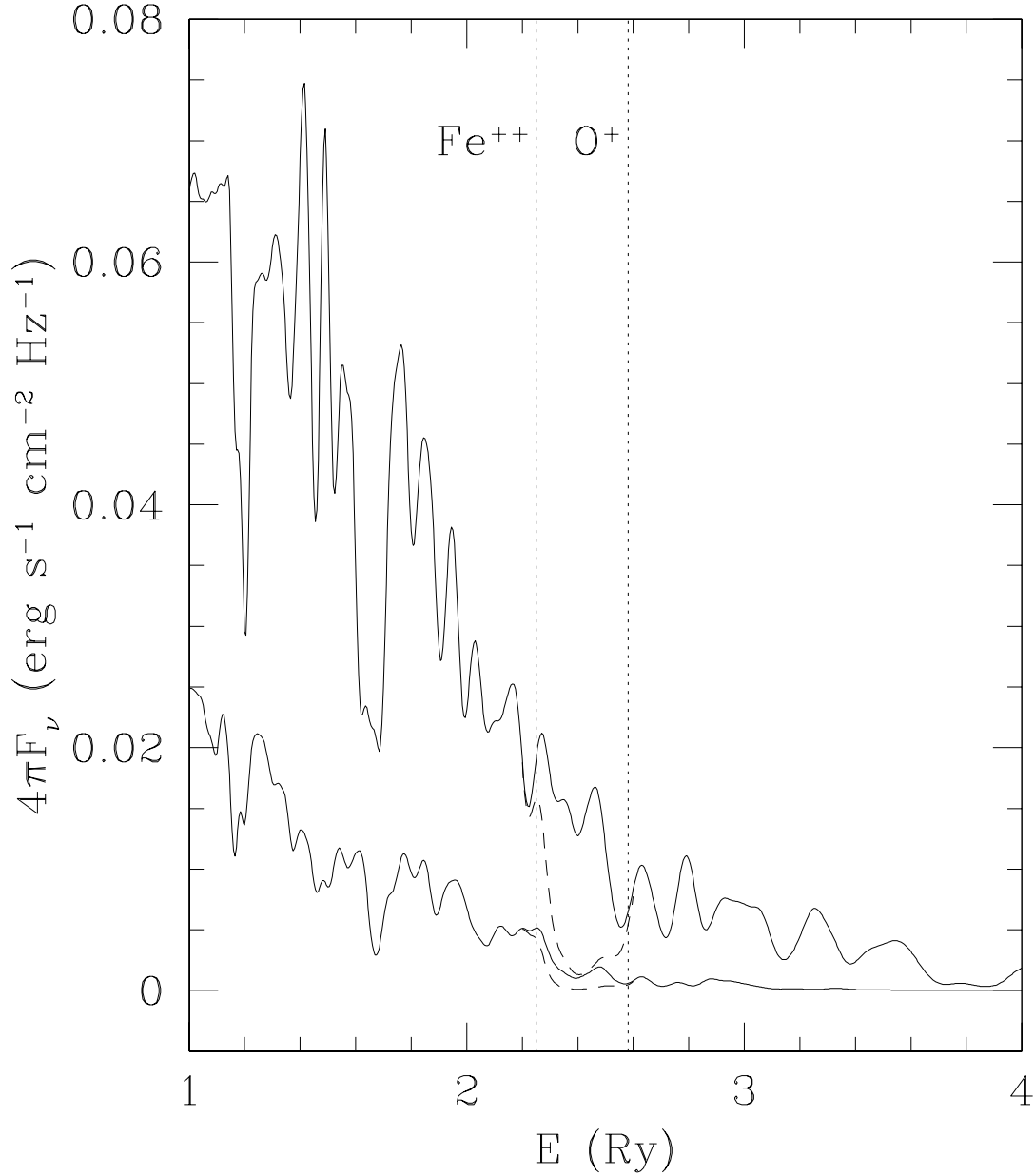


Fig. 4.— *Solid lines*: smoothed model stellar atmosphere spectral energy distributions for $T_{\text{eff}} = 40\,000$ K (lower curve) and $50\,000$ K (upper curve). *Dashed lines*: modified test section of the spectra that we used to check the effect of a lower ionizing flux in the region delimited by the ionization thresholds of O^+ and Fe^{++} (dotted lines). See the text for further information.

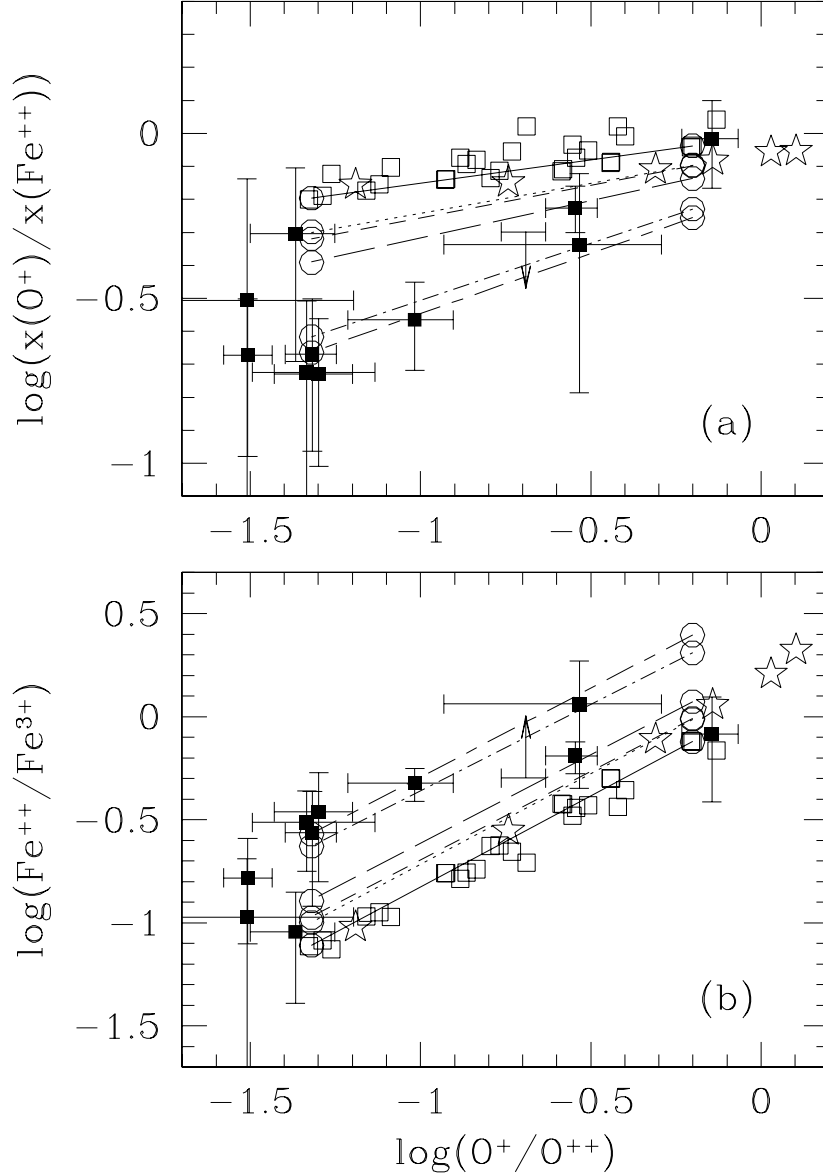


Fig. 5.— Values of $x(O^+)/x(Fe^{++})$ (a) and Fe^{++}/Fe^{3+} (b) as a function of O^+/O^{++} for our new models (open squares and stars, see Fig. 2 for more information) and for the observed objects (filled squares). *Connected open circles*: Predictions from the test models described in §4. From top to bottom in panel (a) and from bottom to top in panel (b): (1) the two models used as templates (connected by a solid line), (2) models with the Fe^{3+} recombination coefficient increased by a factor of 2 (dotted line), (3) models with the rate of the charge exchange reaction $Fe^{3+} + H^0 \rightarrow Fe^{++} + H^+$ increased by a factor of 2 (short dashed line), (4) models with the Fe^{++} ionization cross-section decreased by a factor of 2 (long dashed line), (5) models with the rate of the charge exchange reaction increased by a factor of 10 (dot-dashed line), and (6) models with the Fe^{3+} recombination coefficient increased by a factor of 10 (short-long dashed line).

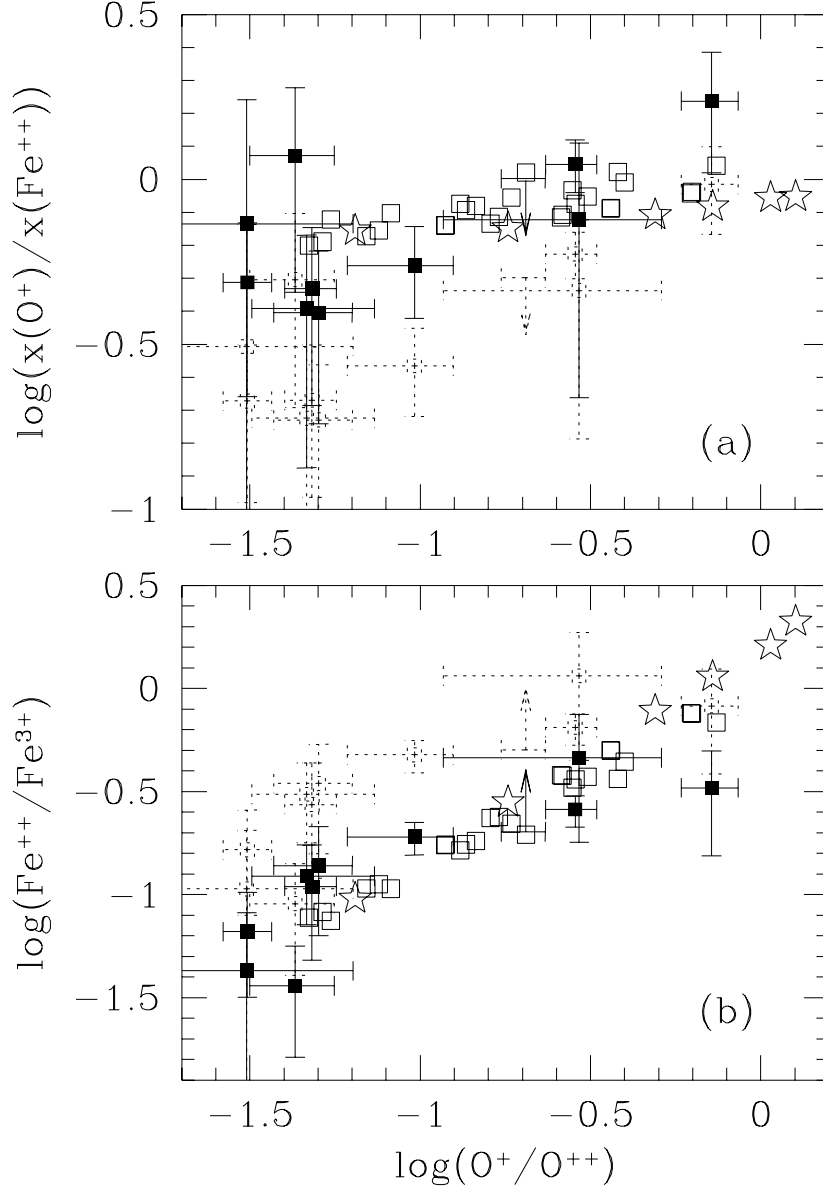


Fig. 6.— Values of $x(O^+)/x(Fe^{++})$ (a) and Fe^{++}/Fe^{3+} (b) as a function of O^+/O^{++} for our new models (open squares and stars, see Fig. 2 for more information) and for the observed objects if the Fe^{3+} abundance is multiplied by a factor of 2.5 or the Fe^{++} abundance is divided by the same factor (filled squares). Dotted lines show the original positions of the observed objects.

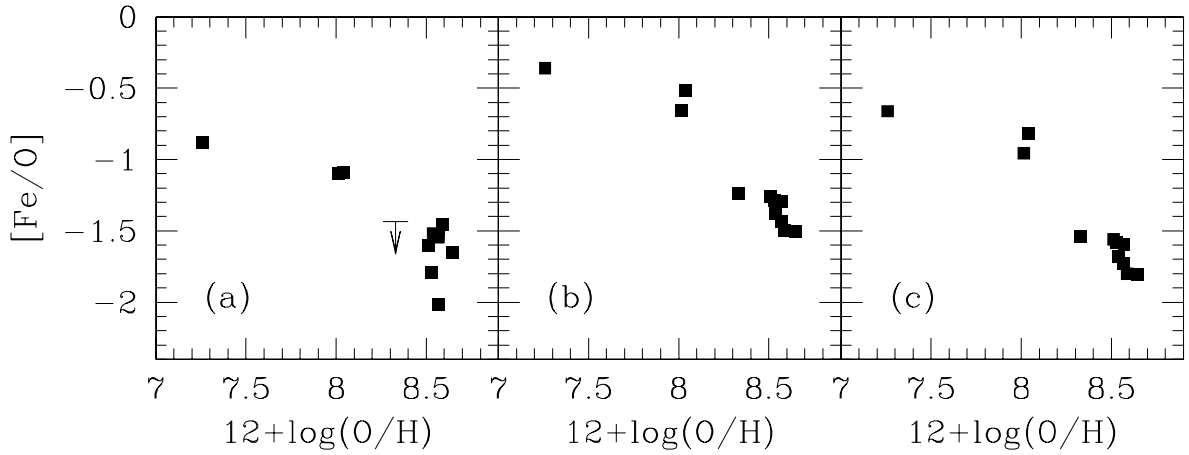


Fig. 7.— Depletion factors ($[\text{Fe}/\text{O}] = \log(\text{Fe}/\text{O}) - \log(\text{Fe}/\text{O})_{\odot}$) for our sample objects as a function of their metallicity given by the O abundance. Panel (a) shows the depletion obtained assuming that both the Fe^{++} and Fe^{3+} collision strengths are approximately correct. Panel (b) shows the results when the Fe^{++} collision strengths and the model predicted concentrations are approximately correct. Panel (c) is for the case where the Fe^{3+} collision strengths and the model predicted concentrations are approximately correct but the Fe^{++} collision strengths are too low by a factor of ~ 2 , leading to Fe^{++} abundances that are too high by a factor of 2.

Table 1. PHYSICAL CONDITIONS

Object	ID	N_e (cm^{-3})	$T_e(\text{low})^a$ (K)	$T_e(\text{high})^a$ (K)	Reference
30 Doradus	LMC H II	440 ± 190	10800^{+350}_{-300}	10000 ± 200	1
IC 4846	Galactic PN	8700 ± 3900	12200^{+5000}_{-2000}	10500^{+900}_{-600}	2
M42 a	Galactic H II	6400 ± 2800	10000^{+1600}_{-1000}	8300^{+600}_{-400}	3
M42 b	Galactic H II	8100 ± 1600	9800^{+300}_{-200}	8300 ± 100	4
N88A bar	SMC H II	10200^{+4800}_{-6100}	14200 ± 400	14200 ± 400	5
N88A sq. A	SMC H II	1500^{+4500}_{-1000}	13500^{+900}_{-600}	13500^{+900}_{-600}	5
NGC 3576	Galactic H II	3000 ± 1200	8500 ± 200	8500 ± 100	6
NGC 6210	Galactic PN	5900 ± 2700	11000^{+400}_{-500}	9600 ± 200	7
NGC 6826	Galactic PN	2300 ± 700	10600 ± 300	9300^{+200}_{-100}	7
NGC 6884	Galactic PN	10200 ± 3700	11200^{+400}_{-300}	11000^{+300}_{-200}	7
SBS 0335–052	H II galaxy	300^{+400}_{-270}	20200^{+800}_{-700}	20200^{+800}_{-700}	8

^a $T_e(\text{low})$ is the T_e derived from the [N II] diagnostic lines; it has been used to derive the O^+ and Fe^{++} abundances. $T_e(\text{high})$ is the T_e implied by the [O III] diagnostic lines; it has been used to derive the O^{++} and Fe^{3+} abundances. $T_e[\text{O III}]$ has been used to derive all ionic abundances in N88A and SBS 0335–052 (Rodríguez 2003).

References. — Line intensities from (1) Peimbert (2003), (2) Hyung, Aller, & Lee (2001), (3) Baldwin et al. (2000), (4) Esteban et al. (2004), (5) Kurt et al. (1999), (6) García-Rojas et al. (2004), (7) Liu et al. (2004a), (8) Izotov et al. (2001).

Table 2. IONIC AND TOTAL ABUNDANCES ($12 + \log X$)

Object	O^+/H^+	O^{++}/H^+	Fe^+/H^+	Fe^{++}/H^+	Fe^{3+}/H^+	O/H	Fe/H ^a	Fe/H ^b
(1)	(2)	(3)	(4)	(5)	(6)	(7)	(8)	(9)
30 Doradus	$7.56^{+0.05}_{-0.06}$	8.25 ± 0.04	...	5.22 ± 0.07	≤ 5.52	8.33 ± 0.03	≤ 5.70	$5.90^{+0.06}_{-0.07}$
IC 4846	$6.99^{+0.31}_{-0.55}$	$8.50^{+0.09}_{-0.12}$...	$4.70^{+0.24}_{-0.60}$	$5.67^{+0.20}_{-0.33}$	$8.51^{+0.09}_{-0.12}$	$5.71^{+0.19}_{-0.29}$	$6.05^{+0.24}_{-0.60}$
M42 a	$7.92^{+0.23}_{-0.32}$	$8.46^{+0.11}_{-0.15}$	4.73:	$5.52^{+0.16}_{-0.20}$	$5.46^{+0.17}_{-0.24}$	$8.57^{+0.10}_{-0.13}$	$5.83^{+0.12}_{-0.13}$	$6.07^{+0.16}_{-0.20}$
M42 b	$7.88^{+0.06}_{-0.08}$	8.43 ± 0.03	4.51: ^c	$5.39^{+0.06}_{-0.07}$	5.58 ± 0.04	$8.54^{+0.02}_{-0.03}$	5.82 ± 0.03	$5.96^{+0.06}_{-0.07}$
N88A bar	$6.96^{+0.11}_{-0.19}$	7.97 ± 0.04	...	5.23 ± 0.05	5.55 ± 0.06	8.01 ± 0.04	5.72 ± 0.04	6.16 ± 0.05
N88A sq. A	$6.69^{+0.19}_{-0.14}$	$8.02^{+0.06}_{-0.08}$...	$5.12^{+0.11}_{-0.15}$	$5.63^{+0.12}_{-0.16}$	$8.04^{+0.06}_{-0.08}$	$5.75^{+0.09}_{-0.12}$	$6.32^{+0.11}_{-0.15}$
NGC 3576	$8.21^{+0.07}_{-0.08}$	8.35 ± 0.03	4.54: ^c	$5.57^{+0.05}_{-0.06}$	$5.65^{+0.18}_{-0.30}$	8.59 ± 0.04	$5.93^{+0.11}_{-0.13}$	$5.89^{+0.05}_{-0.06}$
NGC 6210	$7.26^{+0.11}_{-0.12}$	8.63 ± 0.04	...	4.71 ± 0.08	$5.76^{+0.18}_{-0.32}$	8.65 ± 0.04	$5.79^{+0.17}_{-0.29}$	5.94 ± 0.08
NGC 6826	7.01 ± 0.06	$8.52^{+0.03}_{-0.04}$...	4.69 ± 0.06	$5.47^{+0.18}_{-0.34}$	$8.53^{+0.03}_{-0.04}$	$5.54^{+0.16}_{-0.27}$	6.04 ± 0.06
NGC 6884	$7.25^{+0.09}_{-0.12}$	$8.55^{+0.03}_{-0.04}$...	$4.77^{+0.07}_{-0.08}$	$5.23^{+0.18}_{-0.32}$	$8.57^{+0.03}_{-0.04}$	$5.36^{+0.14}_{-0.21}$	$5.94^{+0.07}_{-0.08}$
SBS 0335-052	$5.92^{+0.06}_{-0.07}$	7.24 ± 0.04	...	4.51 ± 0.11	$5.07^{+0.18}_{-0.31}$	$7.26^{+0.03}_{-0.04}$	$5.18^{+0.15}_{-0.23}$	5.70 ± 0.11

^aDerived from the sum of the ionic abundances.

^bDerived from the Fe^{++} abundance and the *ICF* scheme of equation (2) implied by our photoionization models.

^cDerived using [Fe II] $\lambda 7155$ (see García-Rojas et al. 2004).